

# Safe Navigation in Cluttered Environments Via Spline-Based Harmonic Potential Fields

Theodor-Gabriel Nicu, *Student Member, IEEE*, Florin Stoican, *Member, IEEE*, Daniel-Mihail Ioan, *Member, IEEE*, and Ionela Prodan, *Member, IEEE*

**Abstract**—We provide a complete motion-planning mechanism that ensures target tracking and obstacle avoidance in a cluttered environment. For a given polyhedral decomposition of the feasible space, we adopt a novel procedure that constrains the agent to move only through a prescribed sequence of cells via a suitable control policy.

For each cell, we construct a harmonic potential surface induced by a Dirichlet boundary condition given as a cardinal B-spline curve. A detailed analysis of the curve behavior (periodicity, support) and of the associated control point selection allows us to explicitly compute these harmonic potential surfaces, from which we subsequently derive the corresponding control policy. We illustrate that the resulting construction funnels the agent safely along the chain of cells from the starting point to the target.

**Index Terms**—Artificial Potential Field, Harmonic Functions, Cardinal B-spline Curves, Weighted Graph

## I. INTRODUCTION

Motion planning [17], [9], [13] remains one of the main topics of interest in control theory and autonomous systems. In this context, the *Artificial Potential Field* (APF) approach [14], [24], [23], [16] is both popular and versatile. Broadly speaking, the idea is to construct a potential surface that encodes attraction to the target and repulsion from obstacles, and to apply a control action that drives the system along the negative gradient of this surface. In complex environments, however, trajectories may become trapped in local minima, issue which has spanned multiple approaches. Ad-hoc modifications of the surface, such as adding virtual hills [22] or reactive components [12], often work in practice. Navigation functions are theoretically attractive because they guarantee the existence of a unique, non-degenerate global minimum [14], [11], [25], [15], [18], but this comes at the price of convoluted formulations and conservative tuning parameters.

Another direction, which attempts to sidestep the shortcoming of the global (one-step) methods, is to decompose the motion-planning problem into two independent steps. First, the feasible space is partitioned into a disjoint collection of regions, typically polyhedral [20]; second, one ensures the

Theodor-Gabriel Nicu, Florin Stoican and Daniel Ioan are all with the National University of Science and Technology Politehnica Bucharest, Department of Automatic Control and Systems Engineering and also with the CAMPUS Research Institute (e-mail: theodor.nicu,florin.stoican,daniel.mihail.ioan@upb.ro).

Ionela Prodan is with University Grenoble Alpes, Grenoble INP<sup>†</sup>, LCIS, F-26000, Valence, France (e-mail: ionela.prodan@lcis.grenoble-inp.fr).

transition from one region to the next in such a way that obstacles are avoided and the target is reached. This idea was exploited in [6], [7], which rely on the theory of the Laplace operator (used to describe heat propagation in solids [3], [10]). By constructing a harmonic surface [2], that is, a surface whose Laplacian vanishes in the interior of a region, the surface's minima and maxima are confined to the boundary of that region. Hence, by suitably choosing the boundary conditions, one can force all trajectories entering a given region to exit it in finite time through a particular facet of the polyhedral region. A closed-form solution was first obtained in polar coordinates for the unit disk [8], [5]; a diffeomorphic transformation [26] then mapped this solution to an arbitrary polyhedral set, yielding the formulation detailed in [7].

The caveat of this approach is that the boundary is defined as a piecewise function, which induces sharp changes in the surface gradient near the polyhedron's vertices and imposes restrictive conditions on how the boundary can be specified. Consequently, in our preliminary work [21] we proposed a framework in which the boundary curves are described as weighted sums of cardinal B-splines [19]. The harmonic surfaces derived from these boundary conditions were shown to funnel the agent from the initial point to the target. The sequence of cells was obtained by first modeling a directed graph and subsequently computing the shortest path through it. The current work builds and improves on this scaffolding in several directions:

- i) conditions on periodicity and support for the boundary function are provided, clarifying the tuning parameters involved in its construction;
- ii) a procedure for choosing the control points weighting the cardinal B-spline curve is detailed;
- iii) we generalize the harmonic potential formulation to work for any value of the B-spline order.

The rest of the paper is structured as follows. Section II presents the problem statement. Section III recalls prerequisites on cardinal B-splines. Section IV details the construction of the potential surface from a cardinal B-spline boundary curve, including the harmonic function and control point selection. Section V discusses the resulting control policy and provides an illustrative example. Finally, Section VI summarizes the main conclusions.

## Notations

Let  $\mathbb{X}_{>n} = \{x \in \mathbb{X} : x > n\}$  where  $\mathbb{X}$  is either  $\mathbb{Z}$ , the field of integers, or  $\mathbb{R}$ , the field of reals. For a compact set  $\mathcal{C}$ ,  $\text{int } \mathcal{C}$  stands for its interior and  $\partial \mathcal{C}$  for its boundary.  $\mathcal{F}(\cdot)$  defines the Fourier Transform operator. Operation  $\partial f / \partial x$  denotes the partial derivative of the multi-variate function  $f(\cdot)$  after variable  $x$ . When the function is uni-variate, the operator becomes  $df / dx$ . Notation  $\|x\|$  stands for the standard Euclidian norm applied to a vector  $x \in \mathbb{R}^d$ . For scalar  $x \in \mathbb{R}$ , notations  $\lceil x \rceil, \lfloor x \rfloor \in \mathbb{Z}$  denote the smallest integer larger than  $x$  and the largest integer smaller than  $x$ , respectively.  $\text{sgn}(x)$  returns the sign of scalar  $x \in \mathbb{R}$ .

## II. PROBLEM STATEMENT

Constructing a potential field surface free of spurious local minima and maxima is a challenging task [14], [15], [11]. In this context, harmonic functions, solutions of the Laplace equation on a prescribed domain, are a popular choice [6], as they address the problem in two stages: i) decomposing the free space into a union of cells and ii) prescribing, via local harmonic functions, the behavior within each cell so as to ensure a feasible path from the start point to the destination.

Henceforth, consider a space cluttered with obstacles  $\mathcal{O}_j$ ,

$$\mathbb{R}^2 \setminus \bigcup_j \mathcal{O}_j = \bigcup_\ell P_\ell, \quad (1)$$

decomposed into a collection of polyhedral, non-overlapping regions  $P_\ell$  that form a polyhedral complex [27]. By constraining the agent's trajectory to follow a precomputed sequence of feasible cells  $\{P_{\ell_1} \rightarrow P_{\ell_2} \rightarrow \dots\}$  the agent avoids the obstacles and arrives at the destination.

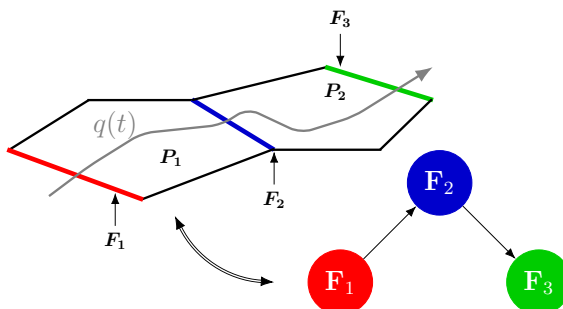


Fig. 1: Proof of concept illustration for the connectivity graph construction

To illustrate this idea, consider two cells,  $P_{1,2}$  and three facets,  $F_{1,2,3}$  chosen such that  $F_1 \in P_1 \setminus P_2$ ,  $F_2 = P_1 \cap P_2$  and  $F_3 = P_2 \setminus P_1$ . Suppose the agent enters  $P_1$  through facet  $F_1$ , transitions into  $P_2$  through  $F_2$ , and exits  $P_2$  through  $F_3$ , as shown in Fig. 1. Repeating this procedure along a prescribed sequence of cells yields trajectories as depicted in Fig. 4.

The remainder of the paper develops a modified harmonic surface construction that guarantees safe transitions between cells, and provides the necessary constructive details along the way.

## III. PRELIMINARIES ON CARDINAL B-SPLINES

To characterize the potential field within each cell, we consider cardinal B-splines whose properties are detailed next.

The cardinal splines  $B_{k,p,\mathbb{Z}}(\theta)$ , of degree  $p \geq 1$ , are obtained recursively from relations

$$M_0(\theta) = \begin{cases} 1, & \forall \theta \in [0, 1], \\ 0, & \text{otherwise,} \end{cases} \quad (2a)$$

$$M_p(\theta) = \frac{\theta}{p} M_{p-1}(\theta) + \frac{p+1-\theta}{p} M_{p-1}(\theta-1), \quad (2b)$$

$$B_{k,p,\mathbb{Z}}(\theta) = B_{0,p,\mathbb{Z}}(\theta-k) = M_p(\theta-k), \quad \forall k \in \mathbb{Z}, \quad (2c)$$

with the properties of (given in their 'local support' form [19]):

**P1** Local support:

$$B_{k,p,\mathbb{Z}}(\theta) = 0, \quad \forall \theta \notin [k, k+p+1]; \quad (3)$$

**P2** Partition of unity:

$$\sum_{k=m-p}^m B_{k,p,\mathbb{Z}}(\theta) = 1, \quad \forall \theta \in [m, m+1]; \quad (4)$$

**P3** The Fourier transform of (2b) is given by

$$\mathcal{F}\{M_p(\theta)\}(\omega) = \left( \frac{1 - e^{-j\omega}}{j\omega} \right)^{p+1}. \quad (5)$$

**P4** The derivative of (2b) is given by

$$\frac{d}{d\theta} M_p(\theta) = M_{p-1}(\theta) - M_{p-1}(\theta-1). \quad (6)$$

The standard cardinal B-spline family (2c) may be scaled with an arbitrary factor  $\lambda \in \mathbb{R}_{>0}$ , to obtain:

$$\sigma_k(\theta) = B_{k,p,\mathbb{Z}}\left(\frac{\theta}{\lambda}\right) = M_p\left(\frac{\theta}{\lambda} - k\right), \quad (7)$$

which, weighted with control points  $P_k$ , gives the B-spline curve

$$h(\theta) = \sum_{k \in \mathbb{Z}} P_k \sigma_k(\theta), \quad \forall \theta \in \mathbb{R}. \quad (8)$$

### Illustrative example

In Fig. 2 we illustrate, for  $p = 3$ , both the seed  $M_\ell(\theta)$  functions, with  $0 \leq \ell \leq p$  computed as in (2a)–(2b) and two of the cardinal B-splines associated with  $M_p(\theta)$ , obtained as in (2c), for  $k \in \{-4, 3\}$ .

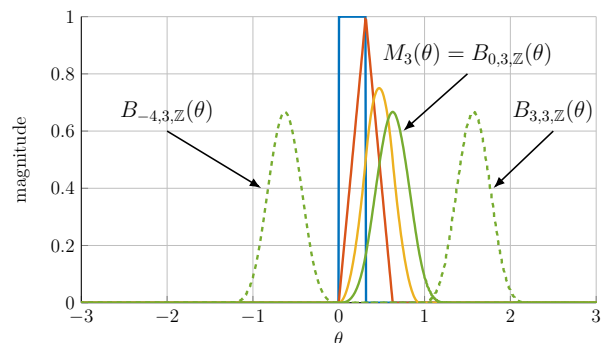


Fig. 2: Cardinal B-splines

#### IV. COMPUTING THE POTENTIAL SURFACE WITH CARDINAL B-SPLINES

The Laplace operator in  $\mathbb{R}^2$  with polar<sup>1</sup> coordinates

$$\nabla^2 = \frac{\partial^2}{\partial r^2} + \frac{1}{r} \frac{\partial}{\partial r} + \frac{1}{r^2} \frac{\partial^2}{\partial \theta^2} \quad (9)$$

ensures that any function  $\gamma(r, \theta)$  defined over a closed region  $\mathcal{C} \subset \mathbb{R}^2$  with non-empty interior, for which

$$\nabla^2 \gamma(r, \theta) = 0, \forall (r, \theta) \in \text{int } \mathcal{C} \quad (10)$$

holds, enjoys two properties of practical importance:

- i)  $\gamma(r, \theta)$  has no points of local minima/maxima (only saddle points),  $\forall (r, \theta) \in \text{int } \mathcal{C}$ ;
- ii) all local minima/maxima of  $\gamma(r, \theta)$  are found on the boundary of its domain:

$$\min / \max_{(r, \theta) \in \mathcal{C}} \gamma(r, \theta) = \min / \max_{(r, \theta) \in \partial \mathcal{C}} \gamma(r, \theta). \quad (11)$$

Taking

$$\mathcal{C} = \{(r, \theta) : r \leq 1, |\theta| \leq \pi\}, \quad (12)$$

as the unit disk, and assuming that the solution over its boundary,  $\partial \mathcal{C} = \{(r, \theta) : r = 1, -\pi \leq \theta \leq \pi\}$ , is known (the “Dirichlet boundary problem”),  $\gamma(r = 1, \theta) = h(\theta)$ , the surface that verifies  $\nabla^2 \gamma(r, \theta) = 0, \forall (r, \theta) \in \text{int } \mathcal{C}$  is

$$\gamma(r, \theta) = A_0 + \sum_{n=1}^{\infty} A_n r^n \cos n\theta + B_n r^n \sin n\theta, \quad (13)$$

where  $A_n, B_n$  come from the trigonometric Fourier series:

$$h(\theta) = A_0 + \sum_{n=1}^{\infty} A_n \cos n\theta + B_n \sin n\theta. \quad (14)$$

While (13) is computed over the unit disk, any map  $\varphi(\cdot)$  that preserves continuity and monotonicity allows to pull it onto an arbitrary convex domain. [6] considers an arbitrary polytope given in half-space representation

$$\mathcal{P} = \{q \in \mathbb{R}^2 : \beta_i(q) \geq 0, \forall i = 1, \dots, m\}, \quad (15)$$

where  $\beta_i(q) = a_i^\top q - b_i$  are linear functions chosen such that  $\mathcal{P}$  is not empty (with shorthand notation  $q = [x \ y]^\top$ ). Then, taking

$$\beta(q) = \beta_{\max}^{\frac{1-m}{m}} \prod_{i=1}^m \beta_i(q), \quad (16)$$

with

$$\beta_{\max} = \prod_{i=1}^m \beta_i(q_\beta), \quad \text{and} \quad q_\beta = \arg \max_q \prod_{i=1}^m \beta_i(q) \quad (17)$$

allows to define the diffeomorphic and monotonous mapping

$$\varphi(q) = \frac{q}{\|q\| + \beta(q)}. \quad (18)$$

Subsequently,  $q \in \mathcal{P} \implies \varphi(q) \in \mathcal{C}$  and, moreover,  $q \in \partial \mathcal{P} \implies \varphi(q) \in \partial \mathcal{C}$ . Thus, we may consider the harmonic potential surface over the polytope  $\mathcal{P}$ , given as

$$\gamma_{\mathcal{P}}(q) = \gamma(\varphi(q)). \quad (19)$$

<sup>1</sup>Variables  $r, \theta$  denote the polar coordinates (radius and angle).

#### A. Computation of the harmonic function

Firstly, we introduce a periodicity condition for  $h(\theta)$  defined as in (8) and characterizing the boundary of  $\mathcal{C}$ .

**Lemma 1:** For a given  $T \in \mathbb{Z}_{>0}$ , let  $\lambda = 2\pi/T$  and  $P_k = P_{k \pm T}$  for all  $k \in \mathbb{Z}$ . Then, the function  $h(\theta)$  defined in (8) satisfies

$$h(\theta) = h(\theta + 2\pi), \quad \forall \theta \in \mathbb{R}. \quad (20)$$

*Proof:* The following chain of equalities holds:

$$\begin{aligned} h(\theta + 2\pi) &\stackrel{(8)}{=} \sum_{k \in \mathbb{Z}} P_k \sigma_k(\theta + 2\pi) \stackrel{(7)}{=} \sum_{k \in \mathbb{Z}} P_k M_p \left( \frac{\theta + 2\pi}{\lambda} - k \right) \\ &\stackrel{\lambda = 2\pi/T}{=} \sum_{k \in \mathbb{Z}} P_k M_p \left( \frac{\theta}{\lambda} + T - k \right) \\ &\stackrel{P_k = P_{k+T}}{=} \sum_{k \in \mathbb{Z}} P_{k+T} M_p \left( \frac{\theta}{\lambda} + T - k - T \right) \\ &= \sum_{k \in \mathbb{Z}} P_{k+T} M_p \left( \frac{\theta}{\lambda} - k \right) = h(\theta), \end{aligned}$$

where, in the last step, a change of variable  $k \mapsto k + T$  is performed. This confirms (20), completing the proof. ■

The next result gives conditions on the indices of the spline functions (7) which do not vanish over the interval  $[0, 2\pi]$ .

**Lemma 2:** The sequence of indices  $k$  whose spline functions  $\sigma_k(\theta)$ , defined as in (7), have supports

- i) fully contained in  $[0, 2\pi]$  is

$$\mathcal{K}_\bullet = \{0, \dots, T - p - 1\}; \quad (21)$$

- ii) partially contained in  $[0, 2\pi]$  is

$$\mathcal{K}_\circ = \{-p, \dots, -1\} \cup \{T - p, \dots, T - 1\}. \quad (22)$$

*Proof:* By property **P1** we have

$$\sigma_k(\theta) = 0, \quad \forall \theta \notin [\lambda k, \lambda(k + p + 1)), \quad (23)$$

which implies that only splines with indices  $k \in \{-p, \dots, T - 1\}$  contribute to the function  $h(\theta)$  on the interval  $[0, 2\pi]$ . Among these, only the indices in (21) correspond to splines whose supports lie entirely within  $[0, 2\pi]$  (i.e., there is no  $\theta \notin [0, 2\pi]$  such that  $\sigma_k(\theta) \neq 0$ ). Subtracting this latter set from the former yields (22), which concludes the proof. ■

We now have the tools to provide the representation of  $h(\theta)$  as a Fourier trigonometric series.

**Proposition 1:** For a sequence of control points respecting

$$P_k = P_{k \pm T}, \quad \forall k \in \mathbb{Z}, \quad P_\ell = 0, \quad \forall \ell \in \mathcal{K}_\circ, \quad (24)$$

with  $\mathcal{K}_\circ$  as in (22) and  $T \in \mathbb{Z}_{>p+1}$ , the Fourier coefficients of the function  $h(\theta)$  are given by relations

$$A_0 = \frac{\lambda}{2\pi} \sum_{k \in \mathcal{K}_\bullet} P_k, \quad (25a)$$

$$A_n = \frac{\lambda}{2\pi(j\lambda n)^{p+1}} \sum_{k \in \mathcal{K}_\bullet} P_k \sum_{\ell=0}^{p+1} (-1)^\ell \binom{p+1}{\ell} E_{n, \ell, k}, \quad (25b)$$

$$B_n = \frac{\lambda}{2\pi(j\lambda n)^{p+1}} \sum_{k \in \mathcal{K}_\bullet} P_k \sum_{\ell=0}^{p+1} (-1)^\ell \binom{p+1}{\ell} F_{n, \ell, k}. \quad (25c)$$

with shorthand notations

$$\begin{aligned} E_{n,\ell,k} &= [1 + (-1)^{p+1}] \cos \lambda n(\ell + k) \\ &\quad - j [1 - (-1)^{p+1}] \sin \lambda n(\ell + k), \end{aligned} \quad (26a)$$

$$\begin{aligned} F_{n,\ell,k} &= j [1 - (-1)^{p+1}] \cos \lambda n(\ell + k) \\ &\quad + [1 + (-1)^{p+1}] \sin \lambda n(\ell + k). \end{aligned} \quad (26b)$$

*Proof:* We start by computing  $\Sigma_k(\omega)$ , the Fourier transform of  $\sigma_k(\theta)$ , from (7), with the help of **P3**:

$$\begin{aligned} \Sigma_k(\omega) &= \mathcal{F}\{\sigma_k(\theta)\} = \mathcal{F}\left\{M_p\left(\frac{\theta}{\lambda} - k\right)\right\} \\ &= \left(\frac{1 - e^{-j\lambda\omega}}{j\lambda\omega}\right)^{p+1} \cdot |\lambda| e^{-j\lambda\omega k}. \end{aligned} \quad (27)$$

Under (24), Lem. 1 ensures that  $h(\theta)$  is  $2\pi$ -periodic and Lem. 2 allows to state that

$$g(\theta) = \sum_{k \in \mathcal{K}_\bullet} P_k \sigma_k(\theta) \quad (28)$$

is the restriction of  $h(\theta)$  on the interval  $[0, 2\pi]$ , i.e., that  $h(\theta) = \sum_{k \in \mathbb{Z}} g(\theta + 2\pi k)$ . Via (27), its Fourier transform is given by

$$G(\omega) = \sum_{k \in \mathcal{K}_\bullet} P_k \left(\frac{1 - e^{-j\lambda\omega}}{j\lambda\omega}\right)^{p+1} \cdot |\lambda| e^{-j\lambda\omega k}. \quad (29)$$

Next, we make use of two results from the folklore of Fourier analysis linking<sup>2</sup>  $h(\theta)$  and  $G(\omega)$ :

i) the coefficients of a Fourier series, given in exponential form ( $D_n$ ) depend on those in trigonometric form ( $A_n, B_n$ ) by

$$D_0 = A_0, \quad D_{\pm n} = \frac{A_n \mp jB_n}{2}, \quad \forall n \geq 1. \quad (30)$$

ii)  $G(\omega)$  verifies

$$D_n = \frac{\omega_0}{2\pi} G(\omega) \Big|_{\omega=n\omega_0} \stackrel{\omega_0=1}{=} \frac{1}{2\pi} G(\omega) \Big|_{\omega=n}. \quad (31)$$

Noting that  $\lambda > 0$  and substituting (29) into (31), we obtain

$$D_n = \frac{1}{2\pi} \sum_{k \in \mathcal{K}_\bullet} \left[ P_k \left(\frac{1 - e^{-j\lambda n}}{j\lambda n}\right)^{p+1} \cdot \lambda e^{-j\lambda n k} \right], \quad (32)$$

which, using (30), yields (25) after a straightforward though tedious manipulation, in which the binomial theorem is applied to expand  $(1 - e^{\mp j\lambda n})^{p+1}$ .

We recall the Taylor series expansion:

$$e^{-x} = 1 - x + \frac{x^2}{2!} - \frac{x^3}{3!} + \frac{x^4}{4!} - \dots$$

from which we obtain the following:

$$\begin{aligned} e^{-j\lambda n} &= 1 - j\lambda n - \frac{\lambda^2 n^2}{2} + \frac{j\lambda^3 n^3}{6} + \frac{\lambda^4 n^4}{24} + \dots \\ 1 - e^{-j\lambda n} &= 1 - 1 + j\lambda n + \frac{\lambda^2 n^2}{2} - \frac{j\lambda^3 n^3}{6} - \frac{\lambda^4 n^4}{24} - \dots \\ \frac{1 - e^{-j\lambda n}}{j\lambda n} &= 1 + \frac{\lambda^2 n^2}{2j\lambda n} - \frac{j\lambda^3 n^3}{6j\lambda n} - \frac{\lambda^4 n^4}{24j\lambda n} - \dots \\ &= 1 + \underbrace{\frac{\lambda n}{2j} - \frac{\lambda^2 n^2}{6} - \frac{\lambda^3 n^2}{24j}}_{n \rightarrow 0} - \dots = 1. \end{aligned}$$

<sup>2</sup>We work under the assumption that  $h(\theta)$  is  $2\pi$ -periodic, hence is fundamental pulsation is  $\omega_0 = 1$ .

Therefore, we have that:

$$\left( \frac{1 - e^{-j\lambda n}}{j\lambda n} \right)^{p+1} \Big|_{n \rightarrow 0} = 1$$

Using this result, we obtain:

$$A_0 = D_0 = \frac{1}{2\pi} \sum_{k \in \mathcal{K}_\bullet} \left[ P_k \cdot \underbrace{\left( \frac{1 - e^{-j\lambda n}}{j\lambda n} \right)^{p+1}}_{=1} \cdot \lambda e^{-j\lambda n k} \right],$$

which means that:

$$A_0 = \frac{\lambda}{2\pi} \sum_{k \in \mathcal{K}_\bullet} P_k$$

Next, we make use of (30) to obtain coefficients  $A_n$  and  $B_n$ .

$$\begin{cases} D_n = \frac{A_n - jB_n}{2} \\ D_{-n} = \frac{A_n + jB_n}{2} \end{cases} \implies A_n = D_n + D_{-n}$$

$$\begin{aligned} A_n &= \frac{1}{2\pi} \sum_{k \in \mathcal{K}_\bullet} \left[ P_k \cdot \left(\frac{1 - e^{-j\lambda n}}{j\lambda n}\right)^{p+1} \cdot \lambda e^{-j\lambda n k} \right] \\ &\quad + \frac{1}{2\pi} \sum_{k \in \mathcal{K}_\bullet} \left[ P_k \cdot \left(\frac{-1 + e^{j\lambda n}}{j\lambda n}\right)^{p+1} \cdot \lambda e^{j\lambda n k} \right] \\ &= \frac{1}{2\pi} \sum_{k \in \mathcal{K}_\bullet} \left[ P_k \frac{1}{(j\lambda n)^{p+1}} \sum_{\ell=0}^{p+1} (-1)^\ell \binom{p+1}{\ell} e^{-j\lambda n \ell} \lambda e^{-j\lambda n k} \right] \\ &\quad + \frac{1}{2\pi} \sum_{k \in \mathcal{K}_\bullet} \left[ P_k \frac{1}{(j\lambda n)^{p+1}} \sum_{\ell=0}^{p+1} (-1)^\ell \binom{p+1}{\ell} e^{j\lambda n \ell} \lambda e^{j\lambda n k} \right] \\ &= \frac{\lambda}{2\pi(j\lambda n)^{p+1}} \sum_{k \in \mathcal{K}_\bullet} \left[ P_k \sum_{\ell=0}^{p+1} (-1)^\ell \binom{p+1}{\ell} e^{-j\lambda n(l+k)} \right] \\ &\quad + \frac{\lambda}{2\pi(j\lambda n)^{p+1}} \sum_{k \in \mathcal{K}_\bullet} \left[ P_k \sum_{\ell=0}^{p+1} (-1)^\ell \binom{p+1}{\ell} e^{j\lambda n(l+k)} \right] \\ &= \frac{\lambda}{2\pi(j\lambda n)^{p+1}} \sum_{k \in \mathcal{K}_\bullet} \left[ P_k \sum_{\ell=0}^{p+1} (-1)^\ell \binom{p+1}{\ell} \left( \cos \lambda n(l+k) - j \sin \lambda n(l+k) \right) \right] \\ &\quad + \frac{\lambda}{2\pi(j\lambda n)^{p+1}} \sum_{k \in \mathcal{K}_\bullet} \left[ P_k \sum_{\ell=0}^{p+1} (-1)^\ell \binom{p+1}{\ell} \left( \cos \lambda n(l+k) + j \sin \lambda n(l+k) \right) \right] \\ &= \frac{\lambda}{2\pi(j\lambda n)^{p+1}} \sum_{k \in \mathcal{K}_\bullet} \left[ P_k \sum_{\ell=0}^{p+1} (-1)^\ell \binom{p+1}{\ell} \cos \lambda n(l+k) \right. \\ &\quad \left. - (-1)^\ell \binom{p+1}{\ell} j \sin \lambda n(l+k) \right] \\ &+ \frac{\lambda}{2\pi(j\lambda n)^{p+1}} \sum_{k \in \mathcal{K}_\bullet} \left[ P_k \sum_{\ell=0}^{p+1} (-1)^{p+1-\ell} \binom{p+1}{\ell} \cos \lambda n(l+k) \right. \\ &\quad \left. + (-1)^{p+1-\ell} \binom{p+1}{\ell} j \sin \lambda n(l+k) \right] \end{aligned}$$

$$\begin{aligned}
&= \frac{\lambda}{2\pi(j\lambda n)^{p+1}} \sum_{k \in \mathcal{K}_\bullet} \left[ P_k \sum_{\ell=0}^{p+1} (-1)^\ell \binom{p+1}{\ell} \left[ \cos \lambda n(l+k) \right. \right. \\
&\quad \left. \left. + (-1)^{p+1} \cos \lambda n(l+k) - j \sin \lambda n(l+k) \right. \right. \\
&\quad \left. \left. + (-1)^{p+1} j \sin \lambda n(l+k) \right] \right] \\
&= \frac{\lambda}{2\pi(j\lambda n)^{p+1}} \sum_{k \in \mathcal{K}_\bullet} \left[ P_k \sum_{\ell=0}^{p+1} (-1)^\ell \binom{p+1}{\ell} \left[ [1 \right. \right. \\
&\quad \left. \left. + (-1)^{p+1}] \cos \lambda n(l+k) - j[1 - (-1)^{p+1}] \sin \lambda n(l+k) \right] \right].
\end{aligned}$$

Therefore,

$$A_n = \frac{\lambda}{2\pi(j\lambda n)^{p+1}} \sum_{k \in \mathcal{K}_\bullet} P_k \sum_{\ell=0}^{p+1} (-1)^\ell \binom{p+1}{\ell} E_{n,\ell,k},$$

where

$$\begin{aligned}
E_{n,\ell,k} &= [1 + (-1)^{p+1}] \cos \lambda n(l+k) \\
&\quad - j[1 - (-1)^{p+1}] \sin \lambda n(l+k).
\end{aligned}$$

Next, for the  $B_n$  coefficient we have that

$$B_n = \frac{A_n - 2D_n}{j} = -j(A_n - 2D_n)$$

Consequently,

$$\begin{aligned}
B_n &= -j \left( \frac{\lambda}{2\pi(j\lambda n)^{p+1}} \sum_{k \in \mathcal{K}_\bullet} P_k \sum_{\ell=0}^{p+1} (-1)^\ell \binom{p+1}{\ell} \right. \\
&\quad \left. \left[ [1 + (-1)^{p+1}] \cos \lambda n(l+k) \right. \right. \\
&\quad \left. \left. - j[1 - (-1)^{p+1}] \sin \lambda n(l+k) \right] \right. \\
&\quad \left. - \frac{2}{2\pi} \sum_{k \in \mathcal{K}_\bullet} \left[ P_k \left( \frac{1 - e^{-j\lambda n}}{j\lambda n} \right)^{p+1} \cdot \lambda e^{-j\lambda n k} \right] \right) \\
&= -j \left( \frac{\lambda}{2\pi(j\lambda n)^{p+1}} \sum_{k \in \mathcal{K}_\bullet} P_k \sum_{\ell=0}^{p+1} (-1)^\ell \binom{p+1}{\ell} \right. \\
&\quad \left. \left[ [1 + (-1)^{p+1}] \cos \lambda n(l+k) \right. \right. \\
&\quad \left. \left. - j[1 - (-1)^{p+1}] \sin \lambda n(l+k) \right] \right. \\
&\quad \left. - \frac{\lambda}{\pi(j\lambda n)^{p+1}} \sum_{k \in \mathcal{K}_\bullet} P_k \sum_{\ell=0}^{p+1} (-1)^\ell \binom{p+1}{\ell} e^{-j\lambda n \ell} e^{-j\lambda n k} \right) \\
&= -j \left( \frac{\lambda}{2\pi(j\lambda n)^{p+1}} \sum_{k \in \mathcal{K}_\bullet} P_k \sum_{\ell=0}^{p+1} (-1)^\ell \binom{p+1}{\ell} \right. \\
&\quad \left. \left[ [1 + (-1)^{p+1}] \cos \lambda n(l+k) \right. \right. \\
&\quad \left. \left. - j[1 - (-1)^{p+1}] \sin \lambda n(l+k) \right] \right. \\
&\quad \left. - \frac{\lambda}{\pi(j\lambda n)^{p+1}} \sum_{k \in \mathcal{K}_\bullet} P_k \sum_{\ell=0}^{p+1} (-1)^\ell \binom{p+1}{\ell} e^{-j\lambda n(\ell+k)} \right)
\end{aligned}$$

$$\begin{aligned}
&= -j \left( \frac{\lambda}{2\pi(j\lambda n)^{p+1}} \sum_{k \in \mathcal{K}_\bullet} P_k \sum_{\ell=0}^{p+1} (-1)^\ell \binom{p+1}{\ell} \right. \\
&\quad \left. \left[ [1 + (-1)^{p+1}] \cos \lambda n(l+k) \right. \right. \\
&\quad \left. \left. - j[1 - (-1)^{p+1}] \sin \lambda n(l+k) \right] \right. \\
&\quad \left. - \frac{\lambda}{\pi(j\lambda n)^{p+1}} \sum_{k \in \mathcal{K}_\bullet} P_k \sum_{\ell=0}^{p+1} (-1)^\ell \binom{p+1}{\ell} \right. \\
&\quad \left. [\cos \lambda n(l+k) - j \sin \lambda n(l+k)] \right) \\
&= \left( \frac{\lambda}{2\pi(j\lambda n)^{p+1}} \sum_{k \in \mathcal{K}_\bullet} P_k \sum_{\ell=0}^{p+1} (-1)^\ell \binom{p+1}{\ell} \right. \\
&\quad \cdot (-j) [[1 + (-1)^{p+1}] \cos \lambda n(l+k) \\
&\quad - j[1 - (-1)^{p+1}] \sin \lambda n(l+k)] \\
&\quad + \frac{\lambda}{2\pi(j\lambda n)^{p+1}} \sum_{k \in \mathcal{K}_\bullet} P_k \sum_{\ell=0}^{p+1} (-1)^\ell \binom{p+1}{\ell} \\
&\quad \cdot (2j) [\cos \lambda n(l+k) - j \sin \lambda n(l+k)] \\
&= \frac{\lambda}{2\pi(j\lambda n)^{p+1}} \sum_{k \in \mathcal{K}_\bullet} P_k \sum_{\ell=0}^{p+1} (-1)^\ell \binom{p+1}{\ell} \\
&\quad \left. \left[ -j \cos \lambda n(l+k) [1 + (-1)^{p+1} - 2] \right. \right. \\
&\quad \left. \left. - [1 - (-1)^{p+1} - 2] \sin \lambda n(l+k) \right] \right).
\end{aligned}$$

Therefore,

$$B_n = \frac{\lambda}{2\pi(j\lambda n)^{p+1}} \sum_{k \in \mathcal{K}_\bullet} P_k \sum_{\ell=0}^{p+1} (-1)^\ell \binom{p+1}{\ell} F_{n,\ell,k},$$

where

$$\begin{aligned}
F_{n,\ell,k} &= j[1 - (-1)^{p+1}] \cos \lambda n(l+k) \\
&\quad + [1 + (-1)^{p+1}] \sin \lambda n(l+k).
\end{aligned}$$

This concludes the proof. ■

For the next result we recall the definition of the polylogarithm  $\text{Li}_{p+1}(z)$  of order  $p+1$ ,

$$\text{Li}_{p+1}(z) = \sum_{n=1}^{\infty} \frac{z^n}{n^{p+1}}. \quad (33)$$

We now have the tools to express  $\gamma(r, \theta)$  as stated next.

*Proposition 2:* With Fourier coefficients (25), (13) becomes

$$\begin{aligned}
\gamma(r, \theta) &= \frac{\lambda}{2\pi} \sum_{k \in \mathcal{K}_\bullet} P_k \left[ 1 + \frac{1}{(j\lambda)^{p+1}} \sum_{\ell=0}^{p+1} (-1)^\ell \binom{p+1}{\ell} \right. \\
&\quad \left. \left( (-1)^{p+1} \text{Li}_{p+1}(re^{j[\lambda(\ell+k)-\theta]}) + \text{Li}_{p+1}(re^{-j[\lambda(\ell+k)-\theta]}) \right) \right], \quad (34)
\end{aligned}$$

*Proof:* Replacing (25) into (13), we arrive at

$$\begin{aligned}
\gamma(r, \theta) &= A_0 + \sum_{n \geq 1} r^n (A_n \cos n\theta + B_n \sin n\theta) \\
&= \frac{\lambda}{2\pi} \sum_{k \in \mathcal{K}_\bullet} P_k + \sum_{n \geq 1} r^n \left( \frac{\lambda}{2\pi(j\lambda n)^{p+1}} \sum_{k \in \mathcal{K}_\bullet} P_k \right. \\
&\quad \left. \sum_{\ell=0}^{p+1} (-1)^\ell \binom{p+1}{\ell} E_{n,\ell,k} \cos n\theta \right. \\
&\quad \left. + \frac{\lambda}{2\pi(j\lambda n)^{p+1}} \sum_{k \in \mathcal{K}_\bullet} P_k \sum_{\ell=0}^{p+1} (-1)^\ell \binom{p+1}{\ell} F_{n,\ell,k} \sin n\theta \right) \\
&= \frac{\lambda}{2\pi} \sum_{k \in \mathcal{K}_\bullet} P_k \sum_{n \geq 1} r^n \left[ \frac{\lambda}{2\pi(j\lambda n)^{p+1}} \sum_{k \in \mathcal{K}_\bullet} P_k \sum_{\ell=0}^{p+1} (-1)^\ell \binom{p+1}{\ell} \right. \\
&\quad \left. \left( E_{n,\ell,k} \cos n\theta + F_{n,\ell,k} \sin n\theta \right) \right] \\
&= \frac{\lambda}{2\pi} \sum_{k \in \mathcal{K}_\bullet} P_k \left[ 1 + \frac{1}{(j\lambda)^{p+1}} \sum_{n \geq 1} \frac{r^n}{n^{p+1}} \right. \\
&\quad \left. \sum_{\ell=0}^{p+1} (-1)^\ell \binom{p+1}{\ell} L_{n,\ell,k,\theta} \right], \quad (35)
\end{aligned}$$

with shorthand notation  $L_{n,\ell,k,\theta}$  given by

$$\begin{aligned}
L_{n,\ell,k,\theta} &= E_{n,\ell,k} \cos n\theta + F_{n,\ell,k} \sin n\theta \\
&= \cos n\theta \left[ [1 + (-1)^{p+1}] \cos \lambda n(l+k) \right. \\
&\quad \left. - j [1 - (-1)^{p+1} \sin \lambda n(l+k)] \right] \\
&\quad + \sin n\theta \left[ j [1 - (-1)^{p+1}] \cos \lambda n(l+k) \right. \\
&\quad \left. + [1 + (-1)^{p+1}] \sin \lambda n(l+k) \right] \\
&= \cos n\theta \cos \lambda n(l+k) [1 + (-1)^{p+1}] \\
&\quad - j \cos n\theta \sin \lambda n(l+k) [1 - (-1)^{p+1}] \\
&\quad + j \sin n\theta \cos \lambda n(l+k) [1 - (-1)^{p+1}] \\
&\quad + \sin n\theta \sin \lambda n(l+k) [1 + (-1)^{p+1}] \\
&= [1 + (-1)^{p+1}] \cos n[\lambda(l+k) - \theta] \\
&\quad - j [1 - (-1)^{p+1}] \sin n[\lambda(l+k) - \theta]. \quad (36)
\end{aligned}$$

Recalling that  $r^n \cos n\phi$  can be written as  $[(re^{j\phi})^n + (re^{-j\phi})^n]/2$  and  $r^n \sin n\phi$  as  $[(re^{j\phi})^n - (re^{-j\phi})^n]/2j$  for  $\phi = \lambda(l+k) - \theta$ , we use (33) and (36) to obtain

$$\begin{aligned}
\sum_{n \geq 1} \frac{r^n}{n^{p+1}} L_{n,\ell,k,\theta} &= \\
\sum_{n \geq 1} \frac{r^n}{n^{p+1}} &\left[ [1 + (-1)^{p+1}] \cos n[\lambda(l+k) - \theta] \right. \\
&\quad \left. - \sum_{n \geq 1} \frac{r^n}{n^{p+1}} j [1 - (-1)^{p+1}] \sin n[\lambda(l+k) - \theta] \right]
\end{aligned}$$

$$\begin{aligned}
&= \sum_{n \geq 1} \frac{r^n}{n^{p+1}} \cos n[\lambda(l+k) - \theta] \\
&\quad + \sum_{n \geq 1} \frac{r^n}{n^{p+1}} (-1)^{p+1} \cos n[\lambda(l+k) - \theta] \\
&\quad - \sum_{n \geq 1} j \frac{r^n}{n^{p+1}} \sin n[\lambda(l+k) - \theta] \\
&\quad + \sum_{n \geq 1} j \frac{r^n}{n^{p+1}} (-1)^{p+1} \sin n[\lambda(l+k) - \theta] \\
&= \sum_{n \geq 1} \frac{r^n}{n^{p+1}} [\cos n[\lambda(l+k) - \theta] - j \sin n[\lambda(l+k) - \theta]] \\
&\quad + (-1)^{p+1} \sum_{n \geq 1} \frac{r^n}{n^{p+1}} [\cos n[\lambda(l+k) - \theta] + j \sin n[\lambda(l+k) - \theta]] \\
&= \sum_{n \geq 1} \frac{r^n}{n^{p+1}} e^{-jn[\lambda(l+k) - \theta]} + (-1)^{p+1} \sum_{n \geq 1} \frac{r^n}{n^{p+1}} e^{jn[\lambda(l+k) - \theta]} \\
&= \sum_{n \geq 1} \frac{(re^{-j[\lambda(l+k) - \theta]})^n}{n^{p+1}} + (-1)^{p+1} \sum_{n \geq 1} \frac{(re^{j[\lambda(l+k) - \theta]})^n}{n^{p+1}} \\
&= (-1)^{p+1} \text{Li}_{p+1}(re^{j[\lambda(l+k) - \theta]}) + \text{Li}_{p+1}(re^{-j[\lambda(l+k) - \theta]}). \quad (37)
\end{aligned}$$

Introducing (37) in (35) leads to (34), thus concluding the proof.  $\blacksquare$

*Remark 1:* Unfortunately, for any  $p > 0$ , (33) defines a transcendental function, i.e., it cannot be expressed in terms of elementary functions. Thus, for practical implementations we resort to approximations of (33). The simplest approach is to truncate the defining series, but more refined methods based on approximations of the zeta function and alternative series representations are also available [4, eq. (27)].  $\blacksquare$

### B. Choosing the control points

To construct the harmonic potential surface in (34), we must appropriately choose the control points  $P_k$  defining the boundary condition (8). The following lemma assists in this.

*Lemma 3:* For scalars  $\theta_0, \theta_1 \in (0, 2\pi)$  with  $\theta_0 < \theta_1$ , take

$$P_k = \begin{cases} -1, & k \in \mathcal{K}_\theta, \\ 0, & \text{otherwise.} \end{cases} \quad (38)$$

where

$$\mathcal{K}_\theta = \left\{ \left\lceil \frac{\theta_0}{\lambda} \right\rceil \leq k \leq \left\lfloor \frac{\theta_1}{\lambda} \right\rfloor - p - 1 \right\}, \quad (39)$$

and

$$\lambda < \frac{\theta_1 - \theta_0}{2(p+1)}. \quad (40)$$

Under these conditions, there exist

$$\theta'_0 = \lambda(\underline{k} + p), \quad \theta'_1 = \lambda\bar{k}, \quad (41)$$

such that  $\theta_0 \leq \theta'_0 < \theta'_1 \leq \theta_1$ , for which  $h(\theta)$  satisfies:

- i)  $h(\theta) = -1$ , for all  $\theta \in [\theta'_0, \theta'_1]$ ;
- ii)  $h(\theta)$  has no local minima outside  $[\theta'_0, \theta'_1]$ .

For later use, we denote

$$\underline{k} = \left\lceil \frac{\theta_0}{\lambda} \right\rceil, \quad \bar{k} = \left\lfloor \frac{\theta_1}{\lambda} \right\rfloor - p. \quad (42)$$

*Proof:* Recalling (23) we have that all indices for which the support of  $\sigma_k(\theta)$  is fully inside the interval  $[\theta_0, \theta_1]$  are those which respect  $\frac{\theta_0}{\lambda} < k < \frac{\theta_1}{\lambda} - p - 1$ , which may be equivalently stated as in (39), where we used the properties  $\lfloor x \pm n \rfloor = \lfloor x \rfloor \pm n$ ,  $\lceil x \pm n \rceil = \lceil x \rceil \pm n$ .

Next, introducing (38) into (8) and applying  $d/d\theta$ , we obtain

$$\begin{aligned} \frac{d}{d\theta} h(\theta) &= -\frac{d}{d\theta} \sum_{k=\underline{k}}^{\bar{k}-1} \sigma_k(\theta) \\ &\stackrel{\text{P4}}{=} -\frac{1}{\lambda} \sum_{k=\underline{k}}^{\bar{k}-1} \left[ M_{p-1}\left(\frac{\theta}{\lambda} - k\right) - M_{p-1}\left(\frac{\theta}{\lambda} - k - 1\right) \right] \\ &= -\frac{1}{\lambda} \left[ M_{p-1}\left(\frac{\theta}{\lambda} - \underline{k}\right) - M_{p-1}\left(\frac{\theta}{\lambda} - \underline{k} - 1\right) \right. \\ &\quad \left. + M_{p-1}\left(\frac{\theta}{\lambda} - \underline{k} - 1\right) - \dots - M_{p-1}\left(\frac{\theta}{\lambda} - \bar{k}\right) \right] \\ &= \frac{1}{\lambda} \left[ -M_{p-1}\left(\frac{\theta}{\lambda} - \underline{k}\right) + M_{p-1}\left(\frac{\theta}{\lambda} - \bar{k}\right) \right]. \end{aligned} \quad (43)$$

Replacing  $p$  with  $p - 1$  in (23) and using that the spline functions  $M_{p-1}(\cdot)$  are positive, we obtain the sign table:

$\theta$	0	$\lambda\underline{k}$	$\lambda(\underline{k} + p)$	$\lambda\bar{k}$	$\lambda(\bar{k} + p)$	$2\pi$
$\text{sgn}\left(\frac{dh(\theta)}{d\theta}\right)$	0	$\cdots$	$0 -$	$\cdots - 0$	$\cdots 0 +$	$\cdots + 0$

The underlying assumption in constructing this table is that the order relations  $0 < \lambda\underline{k} < \lambda(\underline{k} + p) < \lambda\bar{k} < \lambda(\bar{k} + p) < 2\pi$  hold. Using the a priori given notation for  $\underline{k}, \bar{k}$  in (42) and removing redundancies, these conditions reduce to

$$0 < \underline{k}, \quad \bar{k} \leq \left\lceil \frac{2\pi}{\lambda} \right\rceil - p, \quad \underline{k} + p < \bar{k}.$$

which, together with the properties  $\lceil x \rceil \leq x + 1$  and  $\lfloor x \rfloor \geq x - 1$ , lead to the sufficient condition (40).

More precisely,

$$\begin{aligned} \underline{k} + p < \bar{k} &\implies \left\lceil \frac{\theta_0}{\lambda} \right\rceil + p < \left\lfloor \frac{\theta_1}{\lambda} \right\rfloor - p \\ \lceil x \rceil \leq x + 1 &\stackrel{\&}{\implies} \lfloor x \rfloor \geq x - 1 \quad \left\lceil \frac{\theta_0}{\lambda} \right\rceil + p \leq \frac{\theta_0}{\lambda} + 1 + p \\ &< \frac{\theta_1}{\lambda} - 1 - p \leq \left\lfloor \frac{\theta_1}{\lambda} \right\rfloor - p \\ \implies 2(p+1) &< \frac{\theta_1 - \theta_0}{\lambda} \implies \lambda < \frac{\theta_1 - \theta_0}{2(p+1)}. \end{aligned}$$

Furthermore, since  $h(0) = h(2\pi) = 0$  by construction, the sign table shows that the interval on which  $h(\theta) = -1$  is precisely the one in item i), for  $\theta'_0, \theta'_1$  given in (41). Finally, the sign pattern also shows that on this same interval the function attains its minimum and that, outside it, there is no other local minimum, thus verifying item ii) and concluding the proof. ■  
Using the previous result we may now arrive at the final formulation for the harmonic potential surface, one which considers the choice of control points from Lemma 3.

*Corollary 1:* With  $h(\theta)$  from (8) verifying (38)–(41), the harmonic surface (34) becomes

$$\begin{aligned} \gamma(r, \theta) &= -\frac{\lambda(\bar{k} - \underline{k})}{2\pi} - \frac{\lambda}{2\pi(j\lambda)^{p+1}} \sum_{\ell=0}^p (-1)^\ell \binom{p}{\ell} \\ &\quad \left[ (-1)^{p+1} \left( \text{Li}_{p+1}\left(re^{j[\lambda(\ell+\underline{k})-\theta]}\right) - \text{Li}_{p+1}\left(re^{j[\lambda(\ell+\bar{k})-\theta]}\right) \right) \right. \\ &\quad \left. + \text{Li}_{p+1}\left(re^{-j[\lambda(\ell+\underline{k})-\theta]}\right) - \text{Li}_{p+1}\left(re^{-j[\lambda(\ell+\bar{k})-\theta]}\right) \right]. \end{aligned} \quad (44)$$

*Proof:* Introducing into (35) the control points (38) for the index set  $\mathcal{K}_\theta$  defined in (39) under condition (40), and reordering the sums, we arrive at:

$$\begin{aligned} \gamma(r, \theta) &= -\frac{\lambda}{2\pi} \left[ (\bar{k} - \underline{k}) + \frac{1}{(j\lambda)^{p+1}} \sum_{\ell=0}^{p+1} (-1)^\ell \binom{p+1}{\ell} \right. \\ &\quad \left. \sum_{n \geq 1} \frac{r^n}{n^{p+1}} \left( \sum_{k=\underline{k}}^{\bar{k}-1} L_{n,\ell,k,\theta} \right) \right]. \end{aligned} \quad (45)$$

From theory we have that:

$$\sum_{k=0}^{N-1} e^{jkx} = \frac{e^{j0x} - e^{jNx}}{1 - e^{jx}} = \frac{1 - e^{jNx}}{1 - e^{jx}},$$

which leads to:

$$\begin{aligned} \sum_{k=\underline{k}}^{\bar{k}-1} e^{jn[\lambda(l+k)-\theta]} &= \sum_{k=\underline{k}}^{\bar{k}-1} e^{jn\lambda\ell} e^{jn\lambda k} e^{-jn\theta} = e^{jn(\lambda\ell-\theta)} \sum_{k=\underline{k}}^{\bar{k}-1} e^{jn\lambda k} \\ &= e^{jn(\lambda\ell-\theta)} \frac{e^{jn\lambda\underline{k}} - e^{jn\lambda\bar{k}}}{1 - e^{jn\lambda}} = \frac{e^{jn[\lambda(\ell+\underline{k})-\theta]} - e^{jn[\lambda(\ell+\bar{k})-\theta]}}{1 - e^{jn\lambda}}. \end{aligned}$$

For compactness, we note  $\phi = n\lambda$ ,  $\psi = n(\lambda\ell - \theta)$  and obtain

$$\sum_{k=\underline{k}}^{\bar{k}-1} e^{jn[\lambda(l+k)-\theta]} = \sum_{k=\underline{k}}^{\bar{k}-1} e^{j(\phi k + \psi)} = \frac{e^{j(\phi\underline{k} + \psi)} - e^{j(\phi\bar{k} + \psi)}}{1 - e^{j\phi}},$$

which further allows one to write

$$\begin{aligned} \sum_{k=\underline{k}}^{\bar{k}-1} L_{n,\ell,k,\theta} &= \sum_{k=\underline{k}}^{\bar{k}-1} (-1)^{p+1} e^{jn[\lambda(\ell+k)-\theta]} + e^{-jn[\lambda(\ell+k)-\theta]} \\ &= \sum_{k=\underline{k}}^{\bar{k}-1} (-1)^{p+1} e^{j(\phi k + \psi)} + e^{-j(\phi k + \psi)} \\ &= (-1)^{p+1} \sum_{k=\underline{k}}^{\bar{k}-1} e^{j(\phi k + \psi)} + \sum_{k=\underline{k}}^{\bar{k}-1} e^{-j(\phi k + \psi)} \\ &= (-1)^{p+1} \underbrace{\frac{e^{j(\phi\underline{k} + \psi)} - e^{j(\phi\bar{k} + \psi)}}{1 - e^{j\phi}}}_{(*)} + \underbrace{\frac{e^{-j(\phi\underline{k} + \psi)} - e^{-j(\phi\bar{k} + \psi)}}{1 - e^{-j\phi}}}_{(**)} \end{aligned}$$

Tedious but straightforward calculations render term

$$\begin{aligned}
& \sum_{\ell=0}^{p+1} (-1)^\ell \binom{p+1}{\ell} \sum_{n \geq 1} \frac{r^n}{n^{p+1}} \cdot (\star) = \\
& = \sum_{\ell=0}^{p+1} (-1)^\ell \binom{p+1}{\ell} \sum_{n \geq 1} \frac{r^n}{n^{p+1}} \frac{e^{jn[\lambda(\ell+k)-\theta]} - e^{jn[\lambda(\ell+\bar{k})-\theta]}}{1 - e^{jn\lambda}} \\
& = \sum_{\ell=0}^{p+1} (-1)^\ell \binom{p+1}{\ell} \sum_{n \geq 1} \frac{r^n}{n^{p+1}} \frac{e^{jn(\lambda\ell-\theta)}}{1 - e^{jn\lambda}} \left[ e^{jn\lambda k} - e^{jn\lambda \bar{k}} \right] \\
& = \sum_{n \geq 1} \frac{r^n}{n^{p+1}} \frac{e^{-jn\theta}}{1 - e^{jn\lambda}} \left[ e^{jn\lambda k} - e^{jn\lambda \bar{k}} \right] \sum_{\ell=0}^{p+1} e^{jn\lambda \ell} (-1)^\ell \binom{p+1}{\ell} \\
& = \sum_{n \geq 1} \frac{r^n}{n^{p+1}} \frac{e^{-jn\theta}}{1 - e^{jn\lambda}} \left[ e^{jn\lambda k} - e^{jn\lambda \bar{k}} \right] (1 - e^{jn\lambda})^{p+1} \\
& = \sum_{n \geq 1} \frac{r^n e^{-jn\theta}}{n^{p+1}} \left[ e^{jn\lambda k} - e^{jn\lambda \bar{k}} \right] (1 - e^{jn\lambda})^p \quad (46)
\end{aligned}$$

$$\begin{aligned}
& = \sum_{\ell=0}^p (-1)^\ell \binom{p}{\ell} \sum_{n \geq 1} \frac{r^n e^{-jn\theta}}{n^{p+1}} \left[ e^{jn\lambda k} - e^{jn\lambda \bar{k}} \right] e^{jn\lambda \ell} \\
& = \sum_{\ell=0}^p (-1)^\ell \binom{p}{\ell} \sum_{n \geq 1} \frac{r^n}{n^{p+1}} \left[ e^{jn[\lambda(\ell+k)-\theta]} - e^{jn[\lambda(\ell+\bar{k})-\theta]} \right] \\
& = \sum_{\ell=0}^p (-1)^\ell \binom{p}{\ell} \left( \sum_{n \geq 1} \frac{r^n}{n^{p+1}} e^{jn[\lambda(\ell+k)-\theta]} \right. \\
& \quad \left. - \sum_{n \geq 1} \frac{r^n}{n^{p+1}} e^{jn[\lambda(\ell+\bar{k})-\theta]} \right) \\
& = \sum_{\ell=0}^p (-1)^\ell \binom{p}{\ell} \left( \sum_{n \geq 1} \frac{(re^{j[\lambda(\ell+k)-\theta]})^n}{n^{p+1}} - \sum_{n \geq 1} \frac{(re^{j[\lambda(\ell+\bar{k})-\theta]})^n}{n^{p+1}} \right) \\
& = \sum_{\ell=0}^p (-1)^\ell \binom{p}{\ell} \left[ \text{Li}_{p+1} \left( re^{j[\lambda(\ell+k)-\theta]} \right) - \text{Li}_{p+1} \left( re^{j[\lambda(\ell+\bar{k})-\theta]} \right) \right].
\end{aligned}$$

Further noting that  $(\star\star)$  is the conjugate of  $(\star)$  gives

$$\begin{aligned}
& \sum_{\ell=0}^{p+1} (-1)^\ell \binom{p+1}{\ell} \sum_{n \geq 1} \frac{r^n}{n^{p+1}} \cdot (\star\star) \\
& = \sum_{\ell=0}^{p+1} (-1)^\ell \binom{p+1}{\ell} \sum_{n \geq 1} \frac{r^n}{n^{p+1}} \frac{e^{-jn[\lambda(\ell+k)-\theta]} - e^{-jn[\lambda(\ell+\bar{k})-\theta]}}{1 - e^{-jn\lambda}} \\
& = \sum_{\ell=0}^{p+1} (-1)^\ell \binom{p+1}{\ell} \sum_{n \geq 1} \frac{r^n}{n^{p+1}} \frac{e^{-jn(\lambda\ell-\theta)}}{1 - e^{-jn\lambda}} \left[ e^{-jn\lambda k} - e^{-jn\lambda \bar{k}} \right] \\
& = \sum_{n \geq 1} \frac{r^n}{n^{p+1}} \frac{e^{jn\theta}}{1 - e^{-jn\lambda}} \left[ e^{-jn\lambda k} - e^{-jn\lambda \bar{k}} \right] \\
& \quad \cdot \sum_{\ell=0}^{p+1} e^{-jn\lambda \ell} (-1)^\ell \binom{p+1}{\ell} \\
& = \sum_{n \geq 1} \frac{r^n}{n^{p+1}} \frac{e^{jn\theta}}{1 - e^{-jn\lambda}} \left[ e^{-jn\lambda k} - e^{-jn\lambda \bar{k}} \right] (1 - e^{-jn\lambda})^{p+1}
\end{aligned}$$

$$\begin{aligned}
& = \sum_{n \geq 1} \frac{r^n e^{jn\theta}}{n^{p+1}} \left[ e^{-jn\lambda k} - e^{-jn\lambda \bar{k}} \right] (1 - e^{-jn\lambda})^p \\
& = \sum_{\ell=0}^p (-1)^\ell \binom{p}{\ell} \sum_{n \geq 1} \frac{r^n e^{jn\theta}}{n^{p+1}} \left[ e^{-jn\lambda k} - e^{-jn\lambda \bar{k}} \right] e^{-jn\lambda \ell} \\
& = \sum_{\ell=0}^p (-1)^\ell \binom{p}{\ell} \sum_{n \geq 1} \frac{r^n}{n^{p+1}} \left[ e^{-jn[\lambda(\ell+k)-\theta]} - e^{-jn[\lambda(\ell+\bar{k})-\theta]} \right] \\
& = \sum_{\ell=0}^p (-1)^\ell \binom{p}{\ell} \left( \sum_{n \geq 1} \frac{(re^{-j[\lambda(\ell+k)-\theta]})^n}{n^{p+1}} - \sum_{n \geq 1} \frac{(re^{-j[\lambda(\ell+\bar{k})-\theta]})^n}{n^{p+1}} \right) \\
& = \sum_{\ell=0}^p (-1)^\ell \binom{p}{\ell} \left[ \text{Li}_{p+1} \left( re^{-j[\lambda(\ell+k)-\theta]} \right) - \text{Li}_{p+1} \left( re^{-j[\lambda(\ell+\bar{k})-\theta]} \right) \right]. \quad (47)
\end{aligned}$$

Introducing (46) and (47) back into (45) yields (44), thus concluding the proof.  $\blacksquare$

### Illustrative example

To illustrate these constructions, we take  $\lambda = \pi/20$ ,  $p = 3$ , and  $T = 40$ . With  $\theta_0 = 2.52$  and  $\theta_1 = 3.93$ , and applying (38), we obtain in Fig. 3a the function  $h(\theta)$  defined in (8), where we observe the desired behavior: smooth variation and no local minima outside the interval  $[\theta'_0, \theta'_1]$ , with  $\theta'_0 = 3.14, \theta'_1 = 3.45$  as in (41). For better illustration, the cardinal splines are vertically shifted by  $-1$ ; those multiplied by  $P_k = -1$  are shown in blue, while those multiplied by  $P_k = 0$  are shown in light gray.

In Fig. 3b we plot the harmonic potential surface (44), where the polylogarithm functions are approximated by truncating the series (33) after the first 15 terms. We observe that the disk contour follows the wrapped-around  $h(\theta)$  and that the interior surface is free of undesired extrema. Lastly, consider the polyhedral set

$$P = \left\{ q \in \mathbb{R}^2 : \begin{bmatrix} -0.33 & -0.89 \\ 0.28 & -0.69 \\ 0.73 & 0.15 \\ 0.48 & 0.83 \\ -0.58 & 0.65 \\ -0.87 & -0.16 \end{bmatrix} q \geq \begin{bmatrix} 0.28 \\ 0.66 \\ 0.65 \\ 0.28 \\ -0.48 \\ -0.44 \end{bmatrix} \right\}.$$

Using (16)–(17) we obtain  $\beta(q)$  as in (16), which decreases from its maximum at  $\beta_{\max} = 0.04 \cdot 10^{-3}$  from (17) towards zero at the boundary of the polytope. Substituting  $\beta(q)$  into (18) yields the function  $\varphi(q)$ , which maps  $P$  to the unit disk. Selecting the facet with endpoints  $[0.16 \ 0.16]^\top$  and  $[0.23 \ -0.16]^\top$ , we obtain the corresponding values  $\theta_0 = 2.52$  and  $\theta_1 = 3.93$ , the ones used in Figs. 3a–3b, obtained by mapping the facet end-points through  $\varphi(\cdot)$  and putting the result in polar coordinates. With these, we construct the harmonic potential  $\gamma_P(q)$  using (19).

The result is depicted in Fig. 3c, where we observe the desired behavior: the potential surface equals  $h(\varphi(\theta))$  on the boundary and decreases smoothly in the interior so as to “slide” towards the exit facet (the segment in solid red). For illustration, the gradient flow induced by the surface is shown

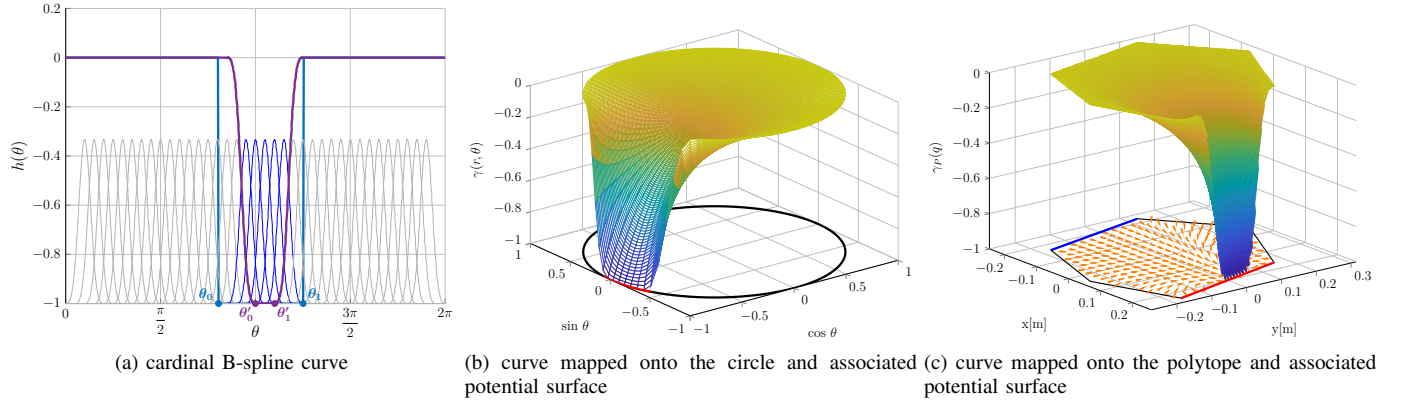


Fig. 3: Mapping of the induced potential surface from the unit disk to the polyhedral case.

in the planar polyhedral cell at the bottom, highlighting that trajectories are constrained to exit through the prescribed facet.

## V. CONTROL POLICY

Consider the double integrator dynamics

$$\ddot{q} = u(q). \quad (48)$$

For single integrator dynamics, a natural control action is to take it proportional to the surface gradient. [6] adapts this to the double integrator case (48) by, first, denoting the normalized negative gradient of the potential (19) as<sup>3</sup>

$$X(q) = -\frac{\nabla_q \gamma_P}{\|\nabla_q \gamma_P\|} = -\frac{\nabla_q^\top \varphi \cdot \nabla_{\varphi(q)} \gamma}{\|\nabla_q^\top \varphi \cdot \nabla_{\varphi(q)} \gamma\|} \quad (49)$$

and, second, its ‘deviation between instantaneous velocity and surface gradient’ as  $\dot{X}(q) = (-\nabla_q X)^\top \dot{q}$ . Put together, these give the control action

$$u(q) = K(X(q) - \dot{q}) + \dot{X}(q), \quad (50)$$

where  $K > 0$  denotes the ‘velocity regulation’.

*Remark 2:* In (50),  $K$  is a proportional gain and its regulation objective is to asymptotically decrease the velocity error,  $e = X(q) - \dot{q}$ , to zero. As stated in [7], the second term in (50) captures the fluctuations in the vector field, allowing to track the integral curves of the normalized gradient (49). ■

Based on (1), we construct the feasible graph  $G = (\mathcal{N}, \mathcal{E})$ , where the nodes enumerate the list of *unique* cell facets that do not appear in the description of any obstacle,

$$\mathcal{N} = \text{unique}\{\mathcal{F}_i \text{ facet of } P_\ell, \forall \ell \wedge \exists j \text{ s.t. } \mathcal{F}_i \in \mathcal{O}_j\}, \quad (51)$$

and the edges, i.e., the facet pairs belonging to a common cell,

$$\mathcal{E} = \{(\mathcal{F}_i, \mathcal{F}_j) : \mathcal{F}_i, \mathcal{F}_j \in \mathcal{N}\}. \quad (52)$$

Applying any *shortest-path* algorithm to link<sup>4</sup> an initial facet  $\mathcal{F}_{\text{start}}$  to a final facet  $\mathcal{F}_{\text{end}}$ , we obtain the sequence

$$\{\mathcal{F}_{k_1}, \dots, \mathcal{F}_{k_M}\} = \text{shortest\_path}(G, \mathcal{F}_{\text{start}}, \mathcal{F}_{\text{end}}). \quad (53)$$

<sup>3</sup>Notation ‘ $\nabla_x \phi$ ’ denotes the gradient of the function ‘ $\phi$ ’ in the variable ‘ $x$ ’ (which may be itself a function, as it happens in the case of composed functions where chain differentiation applies).

<sup>4</sup>For simplicity, we assume that the agent’s start and end positions lie on facets; the extension to arbitrary points is straightforward [7, Sec. 5.2.1].

By construction,  $\mathcal{F}_{k_1} = \mathcal{F}_{\text{start}}$  and  $\mathcal{F}_{k_M} = \mathcal{F}_{\text{end}}$ . The sequence of feasible cell indices corresponding to (53) is obtained as

$$\mathbb{L} = \{\ell_i : \mathcal{F}_{k_i}, \mathcal{F}_{k_{i+1}} \in P_{\ell_i}, \forall i = 1, \dots, M-1\}. \quad (54)$$

Having determined the sequence of cells through which the agent has to pass, we substitute the control action (50) into (48) to arrive at the switched dynamics

$$\ddot{q} = K(X_{\ell_i}(q) - \dot{q}) + \dot{X}_{\ell_i}(q), \quad \forall q \in P_{\ell_i}, \quad (55)$$

where  $X_{\ell_i}(q)$  denotes the normalized gradient corresponding to the harmonic surface associated with cell  $P_{\ell_i}$ . The detailed construction is given next, in Alg. 1.

---

### Algorithm 1 Trajectory computation

---

**Input:** - list of feasible cells  $P_\ell$  and obstacles  $\mathcal{O}_j$ , as in (1);  
- start & end facets ( $\mathcal{F}_{\text{start}}$ ,  $\mathcal{F}_{\text{end}}$ );  
- cardinal B-spline parameters (order  $p$  and scaling factor  $\lambda$ , as used in (2) - (7)).

**Output:** feasible trajectory  $q^*(t)$ , where  $q^*(t) \notin \cup_j \mathcal{O}_j$ ,  $\forall 0 \leq t \leq T_{\text{end}}$ , with  $q^*(0) \in \mathcal{F}_{\text{start}}$  and  $q^*(T_{\text{end}}) \in \mathcal{F}_{\text{end}}$ .

- 1: Construct the feasible graph  $G$ , as in (51)–(52);
- 2: Find shortest path through the graph  $G$  as in (53);
- 3: **for**  $i = 1 : M-1$  **do**
- 4:   select  $\ell_i \in \mathbb{L}$ , as in (54);
- 5:   obtain  $\beta(q)$  as in (16) and  $\varphi(q)$  as in (18), for  $P_{\ell_i}$ ;
- 6:   find  $\theta_0, \theta_1$  such that  $\varphi(F_{k_{i+1}})$  maps the corresponding unit circle arc;
- 7:   get  $\underline{k}, \bar{k}$  as in (42);
- 8:   compute  $\gamma(r, \theta)$  as in (44) and  $\gamma_P(q)$  as in (19);
- 9:   compute control action  $u(q)$  as in (50) and apply it to (48) to obtain closed-loop dynamics (55);
- 10: **end for**
- 11: Integrate the switched closed-loop dynamics (55) to obtain the trajectory  $q^*(t)$ .

---

Note that in Alg. 1 we assume that an environment map is available and that, in a preprocessing step, a classical decomposition algorithm (see, e.g., [20]) is used to generate the list of cells characterizing the free space, as in (1).

### Illustrative Example

Fig. 4 illustrates a cluttered environment with 10 obstacles (red), which induce a partition of the free space (green) into 41 cells forming a polyhedral complex (adjacent cells satisfy the facet-to-facet property [27, Sec. 5.1]). On the same figure, the connectivity graph linking the feasible cells is depicted: 50 markers (blue circles) denote the graph nodes (common facets between adjacent cells), and 77 edges (blue arrows) link all feasible combinations of “in” and “out” facets, as defined in (51)–(52). Note that nodes corresponding to obstacle facets and edges leading to them are considered infeasible and removed from the graph. Thus, implicitly, any path through the graph describes an admissible path for the agent. For illustration, in Fig. 4

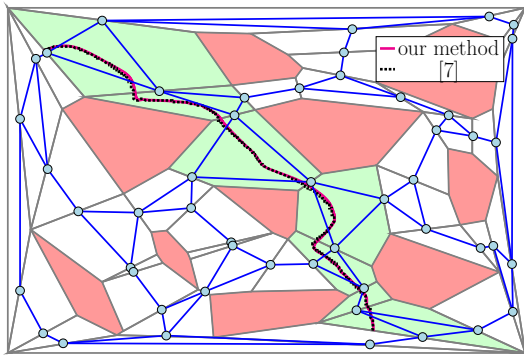


Fig. 4: A cluttered environment, partitioned into polyhedral obstacles and free cells as in (1), overlaid with the facet connectivity graph (51)–(52). Graph nodes are shown at the centroids of the corresponding facets.

a particular path,  $3 \mapsto 1 \mapsto 6 \mapsto 16 \mapsto 17 \mapsto 25 \mapsto 27 \mapsto 28$ , computed as in (53), is obtained by employing the Dijkstra’s shortest path algorithm with the edge cost given by the distance between cell facets. The corresponding agent trajectory is then computed by applying Alg. 1. We observe the desired behavior: the trajectories (solid blue line - our method, dashed blue line - method from [7]) remain within the feasible space, i.e. within the cells composing the path (green) and safely reach the target. The integration time was  $T_{\text{end}} = 25.7$ s and the spline parameters were  $p = 3$  and  $T = 155$ , the latter chosen so that  $\lambda = 2\pi/T$  satisfies the bound 0.0541 obtained from (40). Table I illustrates the link between the unique cell facets (graph nodes) and the polyhedral cells that contain them; except for the initial (start) and final (target) facets, each intermediate facet serves simultaneously as an “out” facet for the preceding cell and an “in” facet for the current cell (the inclusion of a facet within a cell is characterized by the 0/1 flag in the table).

Fig. 5 shows a detail of the construction used in Fig. 4. For three consecutive cells ( $\ell_3 \mapsto \ell_4 \mapsto \ell_5$ ), we highlight the “waterfall” effect, where the harmonic potential surface of each cell funnels the agent so that it slides from one cell to the next through the a priori selected facets.

Lastly, Fig. 6 illustrates the control actions (the *rhs* of (55)), corresponding to the trajectory illustrated in Fig. 4. We observe behavior comparable to [7] in terms of mean and standard deviation for both the norm and the individual components of

		cell index ( $\ell_i \in \mathbb{L}$ , as in (54))						
		1	3	9	10	15	16	17
node index (cell facet, as in (53))	3	1	0	0	0	0	0	0
	1	1	1	0	0	0	0	0
	6	0	1	1	0	0	0	0
	16	0	0	1	1	0	0	0
	17	0	0	0	1	1	0	0
	25	0	0	0	0	1	1	0
	27	0	0	0	0	0	1	1
	28	0	0	0	0	0	0	1

TABLE I: Example of path between nodes 3 and 28

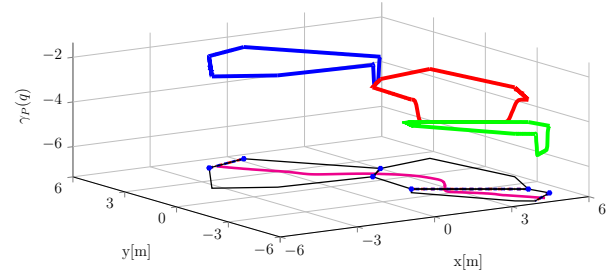


Fig. 5: “Waterfall” effect of the surfaces along a path segment (surfaces and trajectory are vertically shifted for clarity).

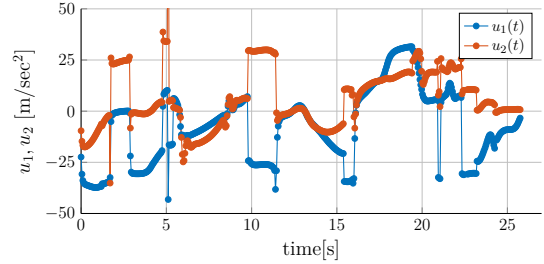


Fig. 6: Control actions (our method)

the control action, as reported in Table II.

Metric	Method	Mean	Std
$\ u\ _2$	Our paper	13.94	11.63
	[7]	13.59	10.91
$u_1$	Our paper	-7.74	18.03
	[7]	-8.29	18.54
$u_2$	Our paper	5.98	15.46
	[7]	4.68	13.18

TABLE II: Input statistics for the example shown in Fig. 4.

The code is available at [gitlab.com/replan/replan-public.git](https://gitlab.com/replan/replan-public.git) in the “Harmonic\_Potential” subdirectory. It makes extensive use of CasADi’s [1] symbolic manipulation and automatic differentiation capabilities.

### VI. CONCLUSIONS

This paper has detailed the constructive underpinnings of a harmonic function-based motion-planning framework, in which the boundary conditions are induced by cardinal B-spline curves. The core contribution is a general treatment

of control point selection, enabling a systematic and flexible design of boundary behavior. This, in turn, yields smooth potential surfaces expressed as harmonic functions over an arbitrary polyhedral decomposition of the configuration space. Future work will focus on further exploiting the richness of spline descriptions (e.g. variable knot vectors and alternative boundary constraints), on clarifying the link between cell decomposition and trajectory performance, and on reducing trajectory variations when transitioning between active cells.

## REFERENCES

- [1] Joel A E Andersson, Joris Gillis, Greg Horn, James B Rawlings, and Moritz Diehl. CasADi – A software framework for nonlinear optimization and optimal control. *Mathematical Programming Computation*, 11(1):1–36, 2019.
- [2] Sheldon Axler, Paul Bourdon, and Ramey Wade. *Harmonic Function Theory*, volume 137. Springer Science & Business Media, 2013.
- [3] Jon Asier Bárcena-Petisco and Enrique Zuazua. Tracking Controllability for the Heat Equation. *IEEE Transactions on Automatic Control*, 2024.
- [4] Vikram Bhagat, Ranjan Bhattacharya, and Dhiranjan Roy. On the evaluation of generalized Bose–Einstein and Fermi–Dirac integrals. *Computer physics communications*, 155(1):7–20, 2003.
- [5] David C Conner, Howie Choset, and Alfred A Rizzi. Flow-Through Policies for Hybrid Controller Synthesis Applied to Fully Actuated Systems. *IEEE Transactions on Robotics*, 25(1):136–146, 2009.
- [6] David C Conner, Alfred A Rizzi, and Howie Choset. Composition of Local Potential Functions for Global Robot Control and Navigation. In *IEEE/RSJ International Conference on Intelligent Robots and Systems*, volume 4, pages 3546–3551. IEEE, 2003.
- [7] David C Conner, Alfred A Rizzi, and Howie M Choset. *Construction and Automated Deployment of Local Potential Functions for Global Robot Control and Navigation*. Carnegie Mellon University, Robotics Institute, 2003.
- [8] Christopher I Connolly, J Brian Burns, and Rich Weiss. Path Planning Using Laplace’s Equation. In *IEEE International Conference on Robotics and Automation*, pages 2102–2106. IEEE, 1990.
- [9] Xiwang Dong, Bocheng Yu, Zongying Shi, and Yisheng Zhong. Time-Varying Formation Control for Unmanned Aerial Vehicles: Theories and Applications. *IEEE Transactions on Control Systems Technology*, 23(1):340–348, 2014.
- [10] Hongyinping Feng and Hai-Li Du. A New Adaptive Control Scheme for Unstable Heat Equation with Unknown Control Coefficient. *IEEE Transactions on Automatic Control*, 2025.
- [11] Ioannis Filippidis and Kostas J Kyriakopoulos. Adjustable Navigation Functions for Unknown Sphere Worlds. In *50th IEEE Conference on Decision and Control and European Control Conference*, pages 4276–4281. IEEE, 2011.
- [12] Haddad Haddad, Maher Khatib, Simon Lacroix, and Raja Chatila. Reactive Navigation in Outdoor Environments using Potential Fields. In *IEEE International Conference on Robotics and Automation*, volume 2, pages 1232–1237. IEEE, 1998.
- [13] George S Kanakis and George A Rovithakis. Motion Planning in Topologically Complex Environments Via Hybrid Feedback. *IEEE Transactions on Automatic Control*, 2024.
- [14] Oussama Khatib. Real-time Obstacle Avoidance for Manipulators and Mobile Robots. In *Autonomous Robot Vehicles*, pages 396–404. Springer, 1986.
- [15] Daniel E Koditschek and Elon Rimon. Robot Navigation Functions on Manifolds with Boundary. *Advances in applied mathematics*, 11(4):412–442, 1990.
- [16] Ro'i Lang and Elon Rimon. Feedback-Based Mobile Robot Navigation in 3-D Environments Using Artificial Potential Functions Technical Report. *arXiv preprint:2601.09318*, 2026.
- [17] Steven M LaValle. *Planning algorithms*. Cambridge University Press, 2006.
- [18] Yueyang Liu, Qinglei Hu, and Gang Feng. Navigation Functions on 3-Manifold With Boundary as a Disjoint Union of Hopf Tori. *IEEE Transactions on Automatic Control*, 70(1):219–234, 2024.
- [19] Tom Lyche, Carla Manni, and Hendrik Speleers. Foundations of Spline Theory: B-Splines, Spline Approximation, and Hierarchical Refinement. In *Splines and PDEs: From Approximation Theory to Numerical Linear Algebra*, pages 1–76. Springer, 2018.
- [20] Cristian Mahulea, Marius Kloetzer, and Ramón González. *Path Planning of Cooperative Mobile Robots Using Discrete Event Models*. John Wiley & Sons, 2020.
- [21] Theodor-Gabriel Nicu, Florin Stoican, Daniel Ioan, and Ionela Prodan. Safe Motion Along Harmonic Potential Surfaces with Cardinal Spline Dirichlet Boundary Conditions. In *IEEE 63rd Conference on Decision and Control*, pages 6578–6583. IEEE, 2024.
- [22] Min Gyu Park and Min Cheol Lee. Real-time Path Planning in Unknown Environment and a Virtual Hill Concept to Escape Local Minima. In *30th Annual Conference of IEEE Industrial Electronics Society*, volume 3, pages 2223–2228. IEEE, 2004.
- [23] Santiago Paternain, Daniel E Koditschek, and Alejandro Ribeiro. Navigation Functions for Convex Potentials in a Space With Convex Obstacles. *IEEE Tran. on Automatic Control*, 63(9):2944–2959, 2017.
- [24] Elon Rimon. *Exact Robot Navigation Using Artificial Potential Functions*. Yale University, 1990.
- [25] Elon Rimon and Daniel E Koditschek. The Construction of Analytic Diffeomorphisms for Exact Robot Navigation on Star Worlds. *Transactions of the American Mathematical Society*, 327(1):71–116, 1991.
- [26] Herbert G Tanner, Savvas G Loizou, and Kostas J Kyriakopoulos. Non-holonomic Navigation and Control of Cooperating Mobile Manipulators. *IEEE Transactions on Robotics and Automation*, 19(1):53–64, 2003.
- [27] Günter M Ziegler. *Lectures on Polytopes*, volume 152. Springer Science & Business Media, 2012.